JOC Article

Distortion, Interaction, and Conceptual DFT Perspectives of MO_4−Alkene (M = Os, Re, Tc, Mn) Cycloadditions

Daniel H. Ess*

The Scripps Research Institute, Scripps Florida, Jupiter, Florida 33458

daniel@scripps.edu

Received October 1, 2008

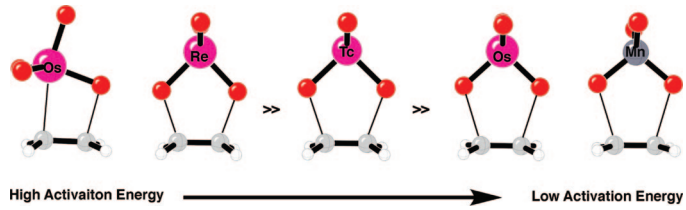

The reaction pathways (including the transition states) of ethylene addition to osmium tetroxide (OsO_4, and amine ligated), rhenate (ReO_4^-), technetate (TcO_4^-), and permanganate (MnO_4^-) have been studied by qualitative and quantitative analyses. Distortion/interaction and absolutely localized energy decomposition analyses provide new insights into why the (3 + 2) pathway is highly preferred over the (2 + 2) pathway, the origin of rate enhancement from ligated base, and reactivity differences between OsO_4, ReO_4^-, TcO_4^-, and MnO_4^-. The (2 + 2) transition state has a much larger barrier than the (3 + 2) transition state because (1) the Os−O bond is stretched significantly resulting in a larger distortion energy ($\Delta E_d^{\ddagger}$) value and (2) the transition state interaction energy ($\Delta E_i^{\ddagger}$) is destabilizing due to large exchange repulsions overwhelming stabilizing charge-transfer terms. Base ligation lowers osmium tetroxide and ethylene distortion energies due to the ground-state O−Os−O angle being predistorted from 110° to 103°. Because MO_4 distortion energies are comparable, reactivity differences between OsO_4, ReO_4^-, TcO_4^-, and MnO_4^- is shown to be a function of ethylene to MO_4 charge-transfer. This interaction also dictates the position of the transition state along the reaction coordinate and corresponds to the onset of a stabilizing $\Delta E_i^{\ddagger}$ value. The conceptual DFT hardness profile and hardness response show that the (3 + 2) reaction pathway may be classified as an "allowed" pathway while the (2 + 2) reaction coordinate is best designated as "forbidden".

Introduction

Metal oxo-mediated oxidation of alkenes is an extremely effective method for installing *cis* vicinal dihydroxy functionality.[1] The reaction of osmium tetroxide (OsO_4), the most commonly used *cis*-dioxo metal reagent, with alkenes has been developed into a widely used catalytic asymmetric version by Sharpless and co-workers.[2] Ruthenium tetroxide (RuO_4)[3−5] and permanganate (MnO_4^-)[6] have been reported to facilitate alkene oxidation.[7] The first step of olefin oxidation, a (3 + 2) cycloaddition to form the osmate ester, the so-called Criegee pathway, has been the subject of controversy (Scheme 1). The direct concerted pathway, akin to the concerted 1,3-dipolar cycloaddition,[8] was the status quo mechanism until Sharpless

(1) Kolb, H. C.; VanNieuwenhze, M. S.; Sharpless, K. B. *Chem. Rev.* **1994**, *94*, 2483.
(2) (a) Criegee, R. *Justus Liebigs Ann. Chem.* **1936**, *522*, 75. (b) Criegee, R.; Marchand, B.; Wannowius, H. *Justus Liebigs Ann. Chem.* **1942**, *550*, 99. (c) Schröder, M. *Chem. Rev.* **1980**, *80*, 187. (d) Jacobsen, E. N.; Markó, I.; Mungall, W. S.; Schröder, G.; Sharpless, K. B. *J. Am. Chem. Soc.* **1988**, *110*, 1968. (e) Ujaque, G.; Maseras, F.; Lledós, A. *J. Am. Chem. Soc.* **1999**, *121*, 1317.
(3) Strassner, T.; Drees, M. *THEOCHEM* **2004**, *671*, 197.
(4) Norrby, P.-O.; Kolb, H. C.; Sharpless, K. B. *Organometallics* **1994**, *13*, 344.
(5) Frunzke, J.; Loschen, C.; Frenking, G. *J. Am. Chem. Soc.* **2004**, *126*, 3642.
(6) (a) Wagner, G. *J. Russ. Phys. Chem. Soc.* **1895**, *27*, 219. (b) Boeseken, J. *Recl. Trav. Chim. Pays-Bas* **1921**, *40*, 553. (c) Wiberg, K. B.; Saegebarth, K. A. *J. Am. Chem. Soc.* **1957**, *79*, 2822. (d) Henbest, H. B.; Jackson, W. R.; Robb, B. C. G. *J. Chem. Soc. B* **1966**, 803. (e) Lee, D. G.; Brownridge, J. R. *J. Am. Chem. Soc.* **1974**, *96*, 5517. (f) Simándi, L. I.; Jáky, M. *J. Am. Chem. Soc.* **1976**, *98*, 1995. (g) Wolfe, S.; Infgold, C. F.; Lemieux, R. U. *J. Am. Chem. Soc.* **1981**, *103*, 938.
(7) Boeseken, J. *Rec. Trav. Chim. Pays-Bas* **1922**, *41*, 199.
(8) (a) Wiberg, K. B.; Geer, R. D. *J. Am. Chem. Soc.* **1966**, *88*, 5827. (b) Huisgen, R. *Angew. Chem. Chem., Int. Ed. Engl.* **1963**, *2*, 565. (c) Huisgen, R. *Angew. Chem. Chem., Int. Ed. Engl.* **1963**, *2*, 633. (d) Huisgen, R. *Angew. Chem. Chem., Int. Ed. Engl.* **1968**, *7*, 321. (e) Huisgen, R. In *1,3-Dipolar Cycloaddition Chemistry*; Padwa, A., Ed.; John Wiley & Sons: New York, 1984; Vol. 1.

10.1021/jo802189w CCC: $40.75
Published on Web 01/13/2009

SCHEME 1. General Metal Oxide Cycloaddition Mechanisms

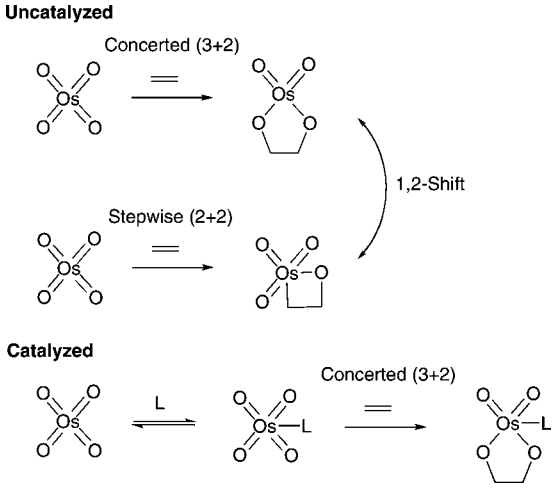

and co-workers favored a stepwise (2 + 2) cycloaddition[9] to give the metallaoxetane[10] followed by rearrangement to the metalladioxo-2,5-dioxolane. Based on observed selectivity and MM2 calculations[11] they postulated a fast and reversible addition of the olefin across the Os═O double bond followed by rate-limiting 1,2-shift (Scheme 1). Diradical mechanisms have also been considered.[12,13] Although experimental data has been reported in support of both concerted[14] and stepwise[15] mechanisms, several quantum mechanical studies have definitively shown that the activation energy necessary for (2 + 2) addition is ∼40 kcal/mol larger than for (3 + 2) addition.[16]

In the ligand (L) catalyzed version, typically amine or bis-amine, there is a pre-equilibrium between osmium tetroxide and base ligation, followed by (3 + 2) addition. The reaction follows Michaelis−Menten kinetics and most nitrogen-based ligands increase the rate. However, quinnuclidine ligands decelerate catalysis because of strong bonding to the osmium(VI) ester intermediate which inhibits turnover by preventing hydrolysis and reoxidation.[17] Mechanistically, Corey has also argued that that a (2 + 2) addition by bis-amine ligated species would involve a 20 electron Os complex, and therefore, a (3 + 2) addition is most likely.[18] Quantum mechanical studies have confirmed that base-assistance does not alter the preference for a concerted reaction pathway, and activation energies are lowered by ∼1−2 kcal/mol.[16]

Despite the several publications describing the transition state (TS) geometries and energies for osmium tetroxide addition to ethylene, as well as the similar rhenate and permanganate TSs, there is surprisingly scant qualitative explanations of reactivity and mechanistic selectivity for these highly important reactions.[16,19] Joergensen and Hoffmann's seminal work using extended Hückel frontier orbitals led to the classification of osmium tetroxide addition to ethylene as a metal-catalyzed forbidden reaction.[20] Frenking and co-workers have more recently used a charge decomposition analysis to compute ratios of orbital donation/back-donation and repulsive interactions that indicate (2 + 2) reaction pathways may be symmetry forbidden.[16f]

In this contribution, several qualitative and quantitative models/analyses are applied to the reaction pathways and transition states of ethylene addition to osmium tetroxide (and amine ligated), rhenate (ReO_4^-), technetate (TcO_4^-), and permanganate (MnO_4^-). section I explores the transition states and intrinsic reaction coordinates of these reactions using the distortion/interaction model that was recently developed for 1,3-dipolar cycloadditions.[21] This model provides insight into the factors controlling the activation energy difference between (3 + 2) and (2 + 2) addition transition states, effects from ligated base, and reactivity differences between OsO_4, ReO_4^-, TcO_4^-, and MnO_4^-. Section II Reports a quantitative transition state interaction energy decomposition for osmium tetroxide (and amine ligated) with ethylene (3 + 2) and (2 + 2) transition states using the absolutely localized molecular orbital decomposition analysis (ALMO-EDA) developed by Head-Gordon and co-workers.[22] Section III applies conceptual DFT descriptors, such as hardness profile,[23] activation hardness,[24] initial hardness response,[25] and the chemical potential profile for the (3 + 2) and (2 + 2) cycloaddition pathways of osmium tetroxide with ethylene.

Computational Methods

All gas phase optimized stationary points were verified as minima or first-order saddle points by calculation of the full Hessian using Gaussian03.[26] All geometries reported are RB3LYP/6-31G(d) (LANL2DZ ECP for Os, Re, Tc, Mn atoms). Mass-weighted intrinsic reaction coordinates (IRC) were followed using the Gonzalez and Schlegel algorithm implemented in Gaussian03 at the default step increment of 0.1 $amu^{1/2}$ bohr. The use of "IRC=CalcAll" ensured force constants were updated for the entire reaction coordinate. For all IRC plots, 19 steps were taken in the

(9) Sharpless, K. B.; Teranishi, A. Y.; Bäckvall, J.-E. *J. Am. Chem. Soc.* **1977**, *99*, 3120.
(10) Jorgensen, K. A.; Schiott, B. *Chem. Rev.* **1990**, *90*, 1483.
(11) Norrby, P.-O.; Kolb, H. C.; Sharpless, K. B. *J. Am. Chem. Soc.* **1994**, *116*, 8470.
(12) (a) Tomioka, K.; Nakajima, M.; Iitaka, Y.; Koga, K. *Tetrahedron Lett.* **1988**, *29*, 573. (b) Tomioka, K.; Nakajima, M.; Koga, K. *Tetrahedron Lett.* **1990**, *31*, 1741.
(13) Ujaque, G.; Maseras, F.; Lledós, A. *Eur. J. Org. Chem.* **2003**, 833.
(14) Corey, E. J.; Noe, M. C. *J. Am. Chem. Soc.* **1996**, *118*, 11038.
(15) (a) Göbel, T.; Sharpless, K. B. *Angew. Chem., Int. Ed. Engl.* **1993**, *32*, 1329. (b) Noorby, P-O.; Gable, K. P. *J. Chem. Soc., Perkin Trans. 2* **1995**, 171.
(16) (a) Veldkamp, A.; Frenking, G. *J. Am. Chem. Soc.* **1994**, *116*, 4937. (b) Dapprich, S.; Ujaque, G.; Maseras, F.; Lledos, A.; Musaev, D. G.; Morokuma, K. *J. Am. Chem. Soc.* **1996**, *118*, 11660. (c) Pidun, U.; Boehme, C.; Frenking, G. *Angew. Chem., Int. Ed. Engl.* **1996**, *35*, 2817. (d) Torrent, M.; Deng, L.; Duran, M.; Sola, M.; Ziegler, T. *Organometallics* **1997**, *16*, 13. (e) DelMonte, A. J.; Haller, J.; Houk, K. N.; Sharpless, K. B.; Singleton, D. A.; Strassner, T.; Thomas, A. A. *J. Am. Chem. Soc.* **1997**, *119*, 9907. (f) Deubel, D. V.; Frenking, G. *J. Am. Chem. Soc.* **1999**, *121*, 2021.
(17) See ref 3. Jacobsen, E. N.; Marko, I.; France, M. B.; Svendsen, J. S.; Sharpless, K. B. *J. Am. Chem. Soc.* **1989**, *111*, 737.
(18) Corey, E. J.; Noe, M. C. *J. Am. Chem. Soc.* **1996**, *118*, 319.
(19) (a) Wu, Y.-D.; Wang, Y.; Houk, K. N. *J. Org. Chem.* **1992**, *57*, 1362. (b) Norrby, P.-O.; Rasmussen, T.; Haller, J.; Strassner, T.; Houk, K. N. *J. Am. Chem. Soc.* **1999**, *121*, 10186.
(20) Joergensen, K. A.; Hoffmann, R. *J. Am. Chem. Soc.* **1986**, *108*, 1867.
(21) (a) Ess, D. H.; Houk, K. N. *J. Am. Chem. Soc.* **2007**, *129*, 10646. (b) Ess, D. H.; Houk, K. N. *J. Am. Chem. Soc.* **2008**, *130*, 10187. (c) Ess, D. H.; Jones, G. O.; Houk, K. N. *Org. Lett.* **2008**, *10*, 1633. (d) Ziegler, T.; Rauk, A. *Theor. Chim. Acta* **1977**, *46*, 1. (e) Ziegler, T.; Rauk, A. *Inorg. Chem.* **1979**, *18*, 1755. (f) Bickelhaupt, F. M.; Ziegler, T.; Schleyer, P. v. R *Organometallics* **1995**, *14*, 2288.
(22) Khaliullin, R. Z.; Cobar, E. A.; Lochan, R. C.; Bell, A. T.; Head-Gordon, M. *J. Phys. Chem. A* **2007**, *111*, 10992.
(23) Datta, D. *J. Phys. Chem.* **1992**, *96*, 2409.
(24) (a) Zhou, Z.; Parr, R. G. *J. Am. Chem. Soc.* **1990**, *112*, 5720. (b) Zhou, Z.; Parr, R. G.; Garst, J. F. *Tetrahedron Lett.* **1988**, *29*, 4843.
(25) (a) De Proft, F.; Ayers, P. W.; Fias, S.; Geerlings, P. *J. Chem. Phys.* **2006**, *125*, 214101. (b) Ayers, P. W.; Morell, C.; De Proft, F.; Geerlings, P. *Chem.—Eur. J.* **2007**, *13*, 8240. (c) De Proft, F.; Chattaraj, P. K.; Ayers, P. W.; Torrent-Sucarrat, M.; Elango, M.; Subramanian, V.; Geerlings, P. *J. Chem. Theory Comput.* **2008**, *4*, 595.
(26) (a) Gaussian03, Revision C.02. Frisch, M. J. et al. Gaussian, Inc.: Wallingford CT, 2004. (see the Supporting Information for the full reference).

forward and reverse directions, except for the reaction pathway for the amine-ligated (2 + 2) addition of ethylene which followed for 31 steps from the transition state to nearly separated reactants. All reported and visualized orbitals are from the Kohn−Sham formalism generated from GaussView.[27] All absolutely localized molecular orbital energy decomposition analysis calculations were performed in Q-Chem 3.1.0.2.[28] The ALMO-EDA method is a variational approach for computing interactions between bimolecular fragments. This method allows the separation of polarization and charge-transfer terms because of an optimized intermediate many-electron state with no electron flow between fragments (see discussion section for further details).[29,30] The 6-31+G(d,p) basis set was used for all ALMO-EDA calculations on geometries obtained from Gaussian03.

Results and Discussion

I. Transition State Distortion/Interaction Analysis. In the late 1990s, there was a flurry of ab initio[16b] and DFT quantum mechanical studies on the mechanism of OsO_4 addition to ethylene.[16] In 1996, Morokuma and co-workers reported an activation barrier ($\Delta E^{\ddagger}$) of 1.9 kcal/mol for formation of the osmate ester (−15.8 kcal/mol) via an amine-free, uncatalyzed (3 + 2) transition state. They reported that the (2 + 2) transition state had a barrier of 43.3 kcal/mol and the osmaoxetane was endothermic by 17.1 kcal/mol. Amine assistance lowered the (3 + 2) barrier to 1.4 kcal/mol and substantially increased the osmate ester exothermicity to −23.5 kcal/mol. The amine-ligated (2 + 2) transition state had a barrier slightly higher than the amine-free pathway (50.4 kcal/mol). In 1997, a seminal collaborative effort by the Singleton, Houk, and Sharpless groups showed that computed kinetic isotope effects can only be reconciled by (3 + 2) addition to form the osmium glycolate primary adduct rather than the osmaoxetane.[16,31]

Although these studies have definitively established that the (3 + 2) transition state is ∼40 kcal/mol lower than the (2 + 2) transition state, the magnitude of activation energy difference is surprising given the fact that Joergensen and Hoffmann could not conclusively determine which reaction pathway and interaction is best based on extended Hückel frontier orbitals.[20] However, Joergensen and Hoffmann did speculate that differences in reactivity might be due to geometric distortion requirements. The distortion/interaction transition state model developed by Ess and Houk provides a highly insightful method for understanding reactivity and activation barriers in cycloadditions.[21] Here the activation energy is dissected into two main components, the distortion ($\Delta E_d^{\ddagger}$) and the interaction ($\Delta E_i^{\ddagger}$) energy (Figure 1). A similar activation strain model has also been developed by Bickelhaupt and co-workers for S_N2 and metal-catalyzed oxidative addition reactions.[32] The distortion energy involves geometric and electronic change to deform the reactants into their transition state geometry. This involves bond stretching, angle decrease or increase, dihedral changes, and

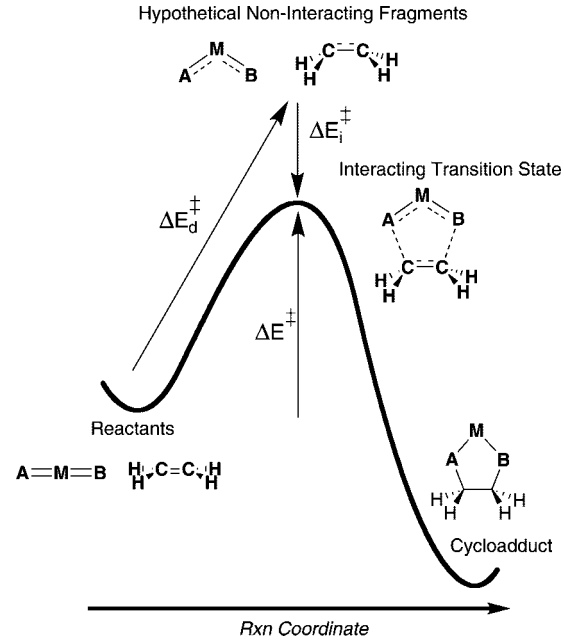

FIGURE 1. Relationship of transition state activation, distortion, and interaction energies.

rehybridization, to name just a few. The interaction energy is comprised of repulsive exchange-repulsions (Pauli repulsions) and stabilizing electrostatic, polarization, and orbital (covalent) effects in the transition state structure. However, in this model, the specific components are not partitioned (see section II). Typically, $\Delta E_d^{\ddagger}$ is directly computed by deletion of each fragment followed by recomputing the remaining fragments energy relative to its optimized structure. The interaction energy is recovered by the relationship: $\Delta E_i^{\ddagger} = \Delta E^{\ddagger} - \Delta E_d^{\ddagger}$.

Figure 2 shows the amine-free and amine-ligated (3 + 2) and (2 + 2) transition states. These transition states have been described elsewhere,[16] and therefore, for brevity only important features are identified. In the C_s-symmetric (3 + 2) addition transition state, **32TS**, the incipient C−O bond lengths are 2.10 Å. The Os−O bonds involved in direct bonding with ethylene are elongated by 0.05 Å, while the two other Os−O bonds remain unchanged. The OOsO bonding angle decreases from 110° in the ground state to 95° in **32TS**. In **22TS**, the single C−O bond is 1.92 Å and the Os−C bond is 2.44 Å. The three OOsO angles are 93°, 119°, and 113°. The ethylene C−C bond length is 0.03 Å longer than in **32TS**.

In the amine-ligated osmium tetroxide, **OsO_4NH_3**, the Os−O bonds are only slightly perturbed, but the OOsO angle decreases to 103°. In the amine-ligated (3 + 2) transition state, **NH_3-32TS**, the C−O bond lengths and the OOsO angle are nearly identical to the amine-free TS.[33] In contrast, the amine-ligated (2 + 2) TS, **NH_3-22TS**, is quite different than **22TS**. Compared

(27) (a) GaussView, Version 3.01. Dennington, R., II.; Keith, T.; Millam, J.; Eppinnett, K.; Hovell, W. L.; Gilliland, R. Semichem, Inc., Shawnee Mission, KS, 2003. (b) All other molecular model figures were generated using Houk mol 2.70: Nakamura, K.; Cheong, P. H.-Y.; Houk, K. N. NAIST and UCLA, 2005.

(28) Q-Chem 3.1.0.2 developmental version. Shao, Y. et al. Q-Chem, Inc., Pittsburgh, PA, 2007 (see the Supporting Information for the full reference).

(29) (a) Mo, Y.; Gao, J.; Peyerimhoff, S. D. *J. Chem. Phys.* **2000**, *112*, 5530. (b) Mo, Y.; Song, L.; Lin, Y. *J. Phys. Chem. A* **2007**, *111*, 8291.

(30) The higher order relaxation term cannot be dissected into directional charge transfer.

(31) Haller, J.; Strassner, T.; Houk, K. N. *J. Am. Chem. Soc.* **1997**, *119*, 8031.

(32) (a) Bickelhaupt, F. M. *J. Comput. Chem.* **1999**, *20*, 114. (b) Velde, G. T.; Bickelhaupt, F. M.; Baerends, E. J.; Guerra, C. F.; Gisbergen, S. J. A. V.; Snijders, J. G.; Ziegler, T. *J. Comput. Chem.* **2001**, *22*, 931. (c) Diefenbach, A.; Bickelhaupt, F. M. *J. Chem. Phys.* **2001**, *115*, 4030. (d) Diefenbach, A.; Bickelhaupt, F. M. *J. Phys. Chem. A* **2004**, *108*, 8460. (e) Diefenbach, A.; Bickelhaupt, F. M. *J. Organomet. Chem.* **2005**, *690*, 2191. (f) Diefenbach, A.; de Jong, G. T.; Bickelhaupt, F. M. *Mol. Phys.* **2005**, *103*, 995. (g) Diefenbach, A.; de Jong, G. T.; Bickelhaupt, F. M. *J. Chem. Theory Comput.* **2005**, *1*, 286. (h) Stralen, J. N. P. v.; Bickelhaupt, F. M *Organometallics* **2006**, *25*, 4260. (i) de Jong, G. T.; Visser, R.; Bickelhaupt, F. M. *J. Organomet. Chem.* **2006**, *691*, 4341. (j) de Jong, G. T.; Bickelhaupt, F. M. *Chem. Phys. Chem.* **2007**, *8*, 1170. (k) de Jong, G. T.; Bickelhaupt, F. M. *J. Chem. Theory Comput.* **2007**, *3*, 514.

(33) NH_3 may occupy two different coordination sites leading to two different transition states. Figure 2 shows only the lowest energy transition state.

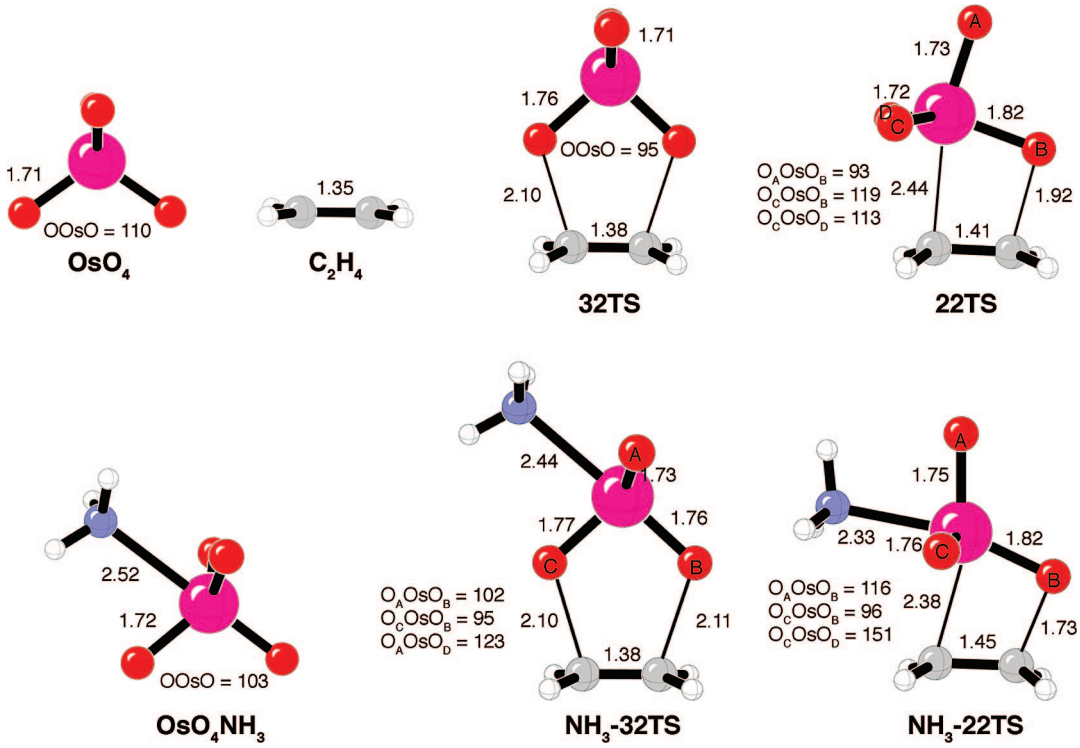

FIGURE 2. OsO_4 cycloaddition transition states.

TABLE 1. Activation, Distortion, and Interaction Transition State Energies for MO_4 Cycloadditions with Ethylene

	$\Delta E^{\ddagger}$ [ΔE rxn]	$\Delta H_{(0K)}{}^{\ddagger}$ [$\Delta H_{(rxn)}$]	$\Delta G_{298}{}^{\ddagger}$	$\Delta E_d{}^{\ddagger}$ (MO_4)	$\Delta E_d{}^{\ddagger}$ (C_2H_4)	$\Delta E_i{}^{\ddagger}$
uncatalyzed						
32TS	4.9 [−33.4]	6.7 [−27.8]	20.1	10.2	4.3	−9.5
22TS	44.9 [6.2]	46.1 [9.3]	56.7	21.3	10.9	12.7
Re-32TS	36.5 [16.1]	38.1 [19.9]	51.4	22.7	16.9	−3.1
Tc-32TS	24.7 [−9.4]			14.1	16.4	−5.7
Mn-32TS	8.7 [−52.1]	9.9 [−8.4]	22.2	4.0	3.5	1.1
catalyzed						
NH_3-32TS	4.2 [−41.0]	6.1 [−35.7]	19.8	5.9	3.9	−5.5
NH_3-22TS	44.7 [14.8]	46.8 [18.0]	61.4	34.1	18.2	−7.6

to **22TS**, the Os−C bond is 0.06 Å shorter and the C−O is 0.19 Å shorter. Overall, the four-centered interaction takes place in a parallelogram (kite)-like structure. The presence of NH_3 alters the OOsO angles up to 40°. As noted in previous publications,[16] the Os−N bond length decreases going from the initial complex to the TS to the cycloadduct.

Table 1 gives the computed activation, distortion, and interaction energies for the transition states in Figure 2. These values correspond well to those previously reported by Morokuma and co-workers and Singleton et al.[16b,e] The (2 + 2) barrier also agrees very well with the CCSD(T) value reported by Frenking and co-workers, but the (3 + 2) barrier is ∼5 kcal/mol lower.[16c] In **32TS**, 10.2 kcal/mol is required to distort OsO_4 and 4.3 kcal/mol is required to distort ethylene. A relaxed energy scan of the OOsO angle in osmium tetroxide shows that angle-only distortion to 95° requires 7.2 kcal/mol (see Figure 8 later). The remaining 3.0 kcal/mol is due to lengthening of the Os−O bonds. An overall stabilizing interaction of −9.5 kcal/mol lowers the barrier a mere 4.9 kcal/mol. The (2 + 2) transition state requires more than twice the amount of energy to distort OsO_4 and ethylene (21.3 and 10.9 kcal/mol, respectively). Although the OOsO angles in **22TS** are very different than in **32TS**, the energy penalty for angle distortion of OsO_4 in **22TS** is 8.5 kcal/mol, surprising similar to the penalty for angle distortion in **32TS**. The remaining 12.8 kcal/mol osmium tetroxide $\Delta E_d{}^{\ddagger}$ is due to Os−O bond stretching, mainly the Os−O directly involved in bond formation. The $\Delta E_d{}^{\ddagger}$ for ethylene is 6.6 kcal/mol larger in **22TS** than in **32TS** and is the result of a later transition-state position; the C−C bond is 0.03 Å longer, and the carbon centers are more pyramidalized. Surprisingly, the interaction energy in this transition state is destabilizing by 12.7 kcal/mol, giving a total barrier of 44.9 kcal/mol. The positive interaction energy must be considered in the context of the mathematical treatment of distortion and interaction energies, that is, the point where $\delta(\Delta E_d{}^{\ddagger}) = -\delta(\Delta E_i{}^{\ddagger})$, which can lead to positive (destabilizing) $\Delta E_i{}^{\ddagger}$ values.[32] However, it is important to note that the frontier interaction between the ethylene HOMO and the osmium metal d-z^2 LUMO orbitals should result in

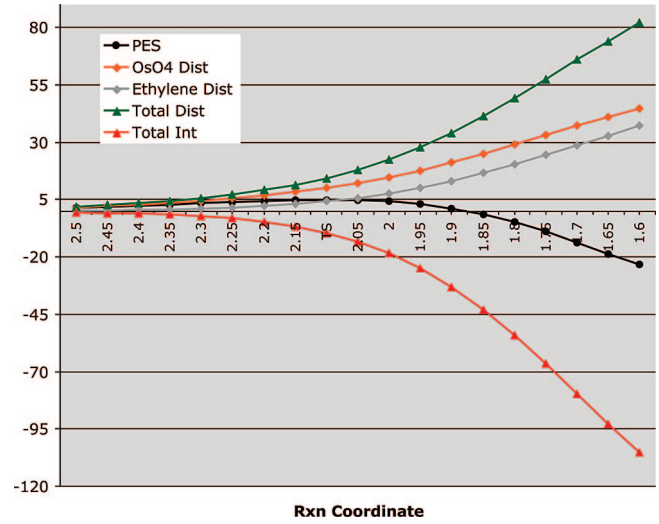

FIGURE 3. Distortion and interaction energy analysis along the C_s reaction coordinate prior to and after **32TS**.

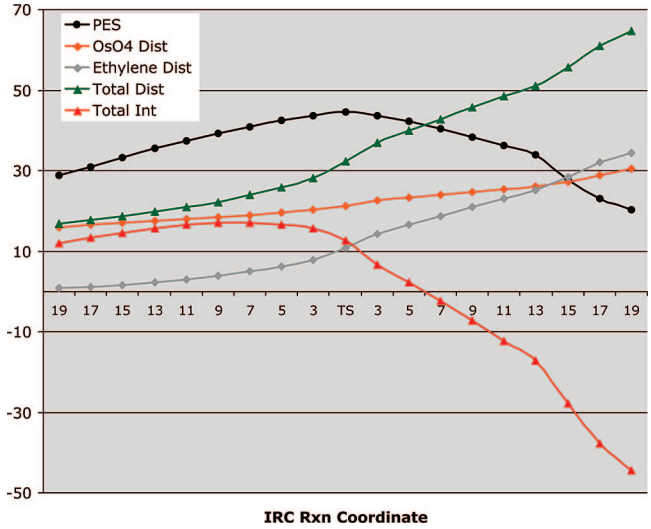

FIGURE 4. Distortion and interaction energy analysis along the intrinsic reaction coordinate 19 steps prior to and 19 steps after **22TS**.

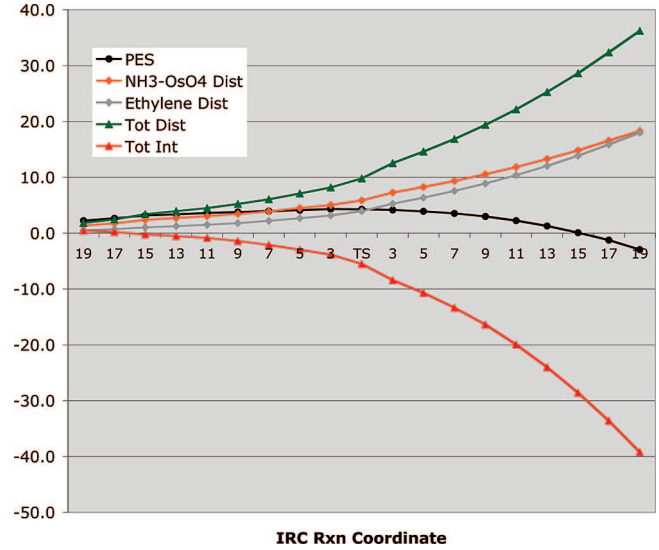

FIGURE 5. Distortion and interaction energy curves along the intrinsic reaction coordinate 19 steps prior to and 19 steps after **NH_3-32TS**.

substantial stabilizing overlap.[20] To understand this surprising result we later decompose this interaction energy into several physically meaningful terms using the absolutely localized molecular orbital method developed by Head-Gordon and coworkers (see section II).[22,28] To summarize, **22TS** has a much larger barrier than **32TS** because (1) the Os−O bond is stretched significantly giving a larger $\Delta E_d^{\ddagger}$ value and (2) $\Delta E_i^{\ddagger}$ is destabilizing. Again, the barriers are not different due to bending of the OOsO angle and dihedral angles.

Figures 3 and 4 show the computed distortion and interaction energies along a C_s symmetric reaction coordinate for (3 + 2) addition and the intrinsic reaction coordinate for (2 + 2). For the (3 + 2) reaction, the C_s reaction coordinate was computed starting from C−O bond lengths of 2.5 Å (close to noninteracting reactants) to 1.6 Å (near the cycloadduct equilibrium). The total distortion and interaction curves look highly similar to those reported for a variety of reactions and increase and decrease respectively in a smooth fashion; the $\Delta E_d^{\ddagger}$ curve increases slightly faster than the $\Delta E_i^{\ddagger}$ curve until the transition state. Throughout the (3 + 2) reaction pathway the OsO_4 distortion energy is always ∼5 kcal/mol larger than ethylene distortion energy. After the TS, the interaction energy curve increases (more negative) much more rapidly, leading to a highly exothermic reaction energy of −33.4 kcal/mol for the cycloadduct.

Figure 4 shows the IRC potential energy surface (PES) before and after **22TS**. Here, the OsO_4 distortion energy increases linearly and therefore the total distortion energy curve mirrors the ethylene distortion energy. Initially there is very little ethylene distortion until near the TS and after it ethylene distortion energy increases rapidly, although not smoothly. At 13 steps after the TS the ethylene distortion curve overtakes the osmium tetroxide distortion. The $\Delta E_i^{\ddagger}$ curve shows only a small linear increase until the TS and after the slope increases dramatically. Initially the interaction energy remains destabilizing by ∼10−15 kcal/mol and does not become stabilizing until 6 IRC steps past the transition state position. Consequently, this is where the total distortion energy curve finally crosses the potential energy curve.

For the (3 + 2) amine-catalyzed transition state, $OsO_4 \cdot NH_3$ requires only 5.9 kcal/mol to achieve the appropriate transition-state geometry. Because the **32TS** and **NH_3-32TS** geometries are nearly identical, this change in distortion energy arises from the ground state OOsO angle being predistorted from 110° to 103°. Ethylene also requires slightly less distortion energy (3.9 kcal/mol). Although amine precoordination lowers $\Delta E_d^{\ddagger}$ by 4.3 kcal/mol, the difference between amine-free and amine-ligated barriers (0.7 kcal/mol) is mitigated by a smaller interaction energy of only −5.5 kcal/mol, resulting in a total activation energy of 4.2 kcal/mol for **NH_3-32TS**.[16d] Therefore, amine rate enhancement is due to lowering the required angle distortion energy via ground-state coordination/predistortion, rather than increasing the total interaction energy in the transition state. Figure 5 shows the distortion and interaction curves for the IRC reaction coordinate of the amine-catalyzed (3 + 2) addition. The curvature and values plotted in Figure 5 are very similar to the uncatalyzed reaction shown in Figure 3 except there is now a small difference between the osmium tetroxide and ethylene distortion energy curves.

The $\Delta E^{\ddagger}$ for **NH_3-22TS** is 0.2 kcal/mol higher in energy than **22TS**. However, the computed $\Delta E_d^{\ddagger}$ and $\Delta E_i^{\ddagger}$ values are significantly different. In **NH_3-22TS**, $OsO_4 \cdot NH_3$ requires 34.1 kcal/mol to achieve the transition-state geometry because the amine coordination substantially stabilizes the ligand arrangement and biases the ability of OsO_4 to distort by decreasing the OOsO angle. Although **NH_3-22TS** requires substantially more distortion energy, the interaction energy is now stabilizing by −7.6 kcal/mol. Figure 6 shows plots of the distortion and interaction energies along the IRC prior to **NH_3-22TS**. Similar to the uncatalyzed reaction, the interaction energy initially has a positive slope. However, the slope changes from positive to negative at ∼17 steps prior to the transition state. This leads to the interaction energy becoming stabilizing just prior to the transition state and the total distortion energy crossing the PES curve at this point.

Table 1 also reports the computed TS distortion and interaction energies for the (3 + 2) cycloaddition transition states of

(34) (a) Pietsch, M. A.; Russo, T. V.; Murphy, R. B.; Martin, R. L.; Rappé, A. K. *Organometallics* **1998**, *17*, 27160. (b) Deubel, D. V.; Frenking, G. *J. Am. Chem. Soc.* **2001**, *123*, 10085.

(35) (a) Deubel, D. V.; Frenking, G. *Acc. Chem. Res.* **2003**, *36*, 645. (b) Deubel, D. V.; Schlecht, S.; Frenking, G. *J. Am. Chem. Soc.* **2001**, *123*, 10085.

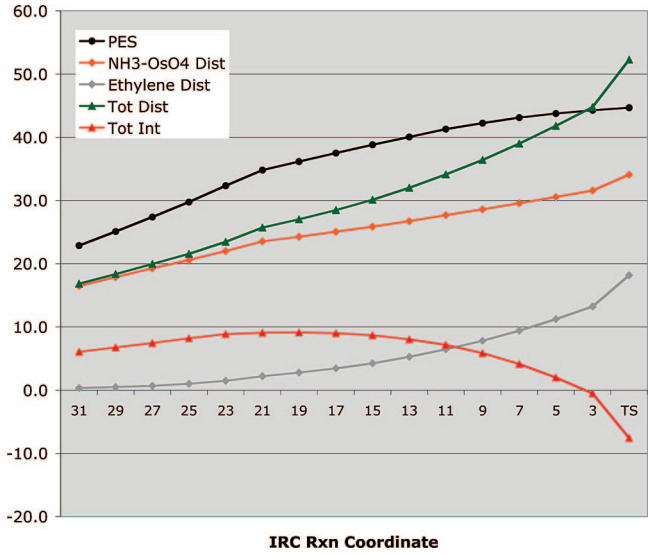

FIGURE 6. Distortion and interaction energy curves along the intrinsic reaction coordinate 31 steps prior to **NH_3-22TS**.

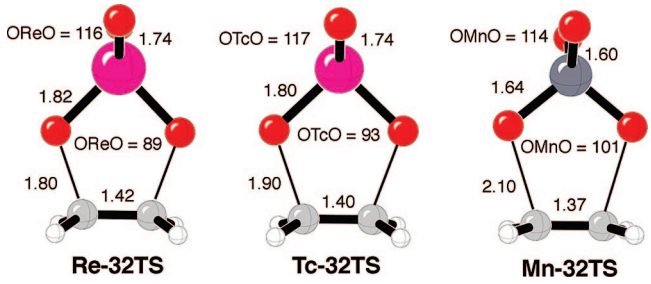

FIGURE 7. Rhenate, technetate, and permanganate (3 + 2) transition states.

anionic metal oxo complexes rhenate (**Re-32TS**),[34−36] technetate (**Tc-32TS**), and permanganate (**Mn-32TS**) (Figure 7). Previous DFT studies have also shown that these oxidants undergo preferred (3 + 2) addition.[37−39]

Although the ReO_4^- anionic *cis*-dioxo complex is isoelectronic with OsO_4, the activation energy for **Re-32TS** is surprisingly large ($\Delta E^{\ddagger} = 36.5$ kcal/mol). This is consistent with Gable et al. showing that pentamethyl cyclopentadienyl trioxorhenium(VII) only reacts with strained alkenes.[40] The barrier for addition decreases to 24.7 kcal/mol for **Tc-32TS** and to 8.7 kcal/mol for **Mn-32TS**. The reaction energies likewise increase from 16.1 to −9.4 to −52.1 kcal/mol. As the $\Delta E^{\ddagger}$ decreases, the corresponding increase in reaction energies has previously been discussed by Gisdakis and Rösch in terms of Marcus theory.[41] The large activation energy for ReO_4^- is the result of a severe energy penalty to distort ReO_4^- and results in a $\Delta E_d^{\ddagger}$ value of 22.7 kcal/mol for rhenate and 16.9 kcal/mol for ethylene. The interaction between rhenate and ethylene fragments is only −3.1 kcal/mol, resulting in an overall barrier of 36.5 kcal/mol. In **Tc-32TS**, 14.1 kcal/mol of energy is required

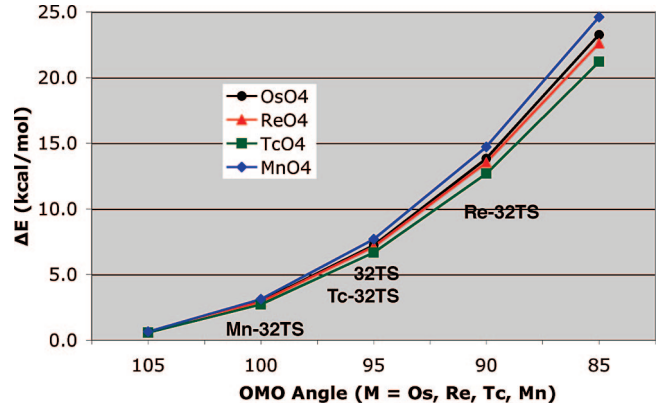

FIGURE 8. Relative angle distortion energies for osmium tetroxide, rhenate, technetate, and permanganate (kcal/mol). The approximate position of the transition state is indicated.

to distort TcO_4^- and 16.4 kcal/mol for ethylene. A −5.7 kcal/mol interaction energy gives a total activation energy of 24.7 kcal/mol. In the permanganate TS, the required distortion energy (4.0 for MnO_4^- and 3.5 kcal/mol for C_2H_4) is actually smaller than that for the osmium tetroxide (3 + 2) TS. However, the (3 + 2) permanganate TS has a destabilizing interaction energy of 1.1 kcal/mol, resulting in a barrier of 8.7 kcal/mol.

The transition state distortion energies suggest that rhenate has a large barrier due to large distortion energies. Although this is true, there are significant geometrical differences between all the (3 + 2) transition states. The C−O bond lengths and the OReO angle (89°) in **Re-32TS** indicate a very late transition state. Also, the C−C bond length of ethylene is stretched to 1.42 Å and the carbon centers are significantly pyramidalized. The OOsO and OMnO angles and C−C bond lengths for **32TS** and **Mn-32TS** suggest much earlier TSs. Because the position of the (3 + 2) transition states differ along the C−O bond and OMetalO angle reaction coordinates, computing the transition state distortion energies cannot directly determine whether the intrinsic stability of each metal oxo complex, as determined by $\Delta E_d^{\ddagger}$, controls the barrier heights. Figure 8 shows relaxed potential energy surface scans for the OMO angles of osmium tetroxide, rhenate, technetate, and permanganate. Surprisingly, the energy penalty to deform the OMetalO angle for these species is very similar. This indicates that the barrier heights are *not* controlled by relative angle distortion energies but rather the combination of the M−O bond distortion energy and the ethylene distortion energy as dictated by the position along the reaction coordinate based on interaction energies. Because the OMO angle distortion energies are similar, there is a resulting correlation between activation energies and reaction energies and metal-oxo bond dissociation energies.[41]

To understand the similar bending energies of these metal oxo complexes, Figure 9 shows the most important Kohn−Sham occupied and unoccupied osmium tetroxide and rhenate orbitals and their energies as the OMO angles are decreased. There are only small changes in orbital energies prior to the TS because the important occupied orbitals are essentially nonbonding lone pairs centralized on the oxygen atoms with little or no contribution from the metal center. Therefore, bending in a C_s symmetric fashion requires similar polarization via HOMO−LUMO mixing, despite the very different metal centers. The HOMO−LUMO gap of OsO_4 and ReO_4^- remain approximately constant at 5.4 and 6.4 eV, respectively.

Although the HOMO−LUMO gaps of the MO_4 species are similar, the LUMO energy and the extent of the interaction with

(36) Haller, J.; Beno, B. R.; Houk, K. N. *J. Am. Chem. Soc.* **1998**, *120*, 6468.
(37) (a) Houk, K. N.; Strassner, T. *J. Org. Chem.* **1999**, *64*, 800. (b) Wiberg, K. B.; Wang, Y.-g.; Sklenak, S.; Deutsch, C.; Trucks, G *J. Am. Chem. Soc.* **2006**, *128*, 11537.
(38) (a) Torrent, M.; Deng, L.; Ziegler, T. *Inorg. Chem.* **1998**, *37*, 1307. (b) Torrent, M.; Deng, L.; Duran, M.; Sola, M.; Ziegler, T *Can. J. Chem.* **1999**, *77*, 1476.
(39) Strassner, T.; Busold, M. *J. Phys. Chem. A* **2004**, *108*, 4455.
(40) Gable, K. P.; Juliett, J. J. J. *J. Am. Chem. Soc.* **1994**, *116*, 833.
(41) Gisdakis, P.; Rösch, N. *J. Am. Chem. Soc.* **2001**, *123*, 697.

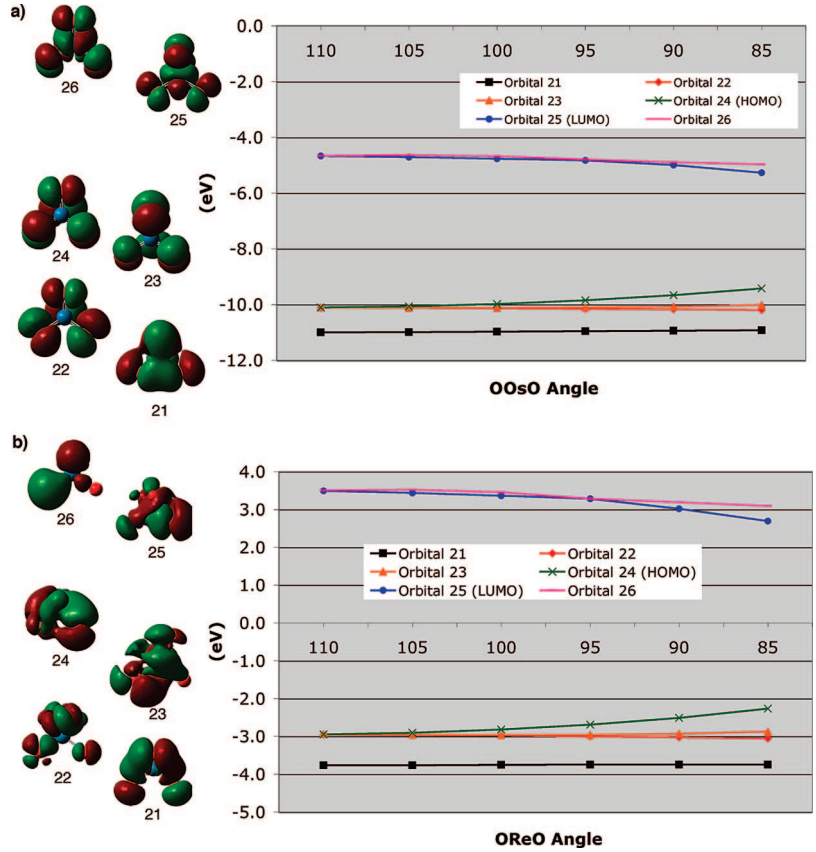

FIGURE 9. Orbital energy changes as OMO angle decreases for (a) OsO_4 and (b) ReO_4^-.

the ethylene HOMO orbital is very different (see section II). The rhenate$_{LUMO}$−ethylene$_{HOMO}$ gap is nearly 7 eV greater than the same frontier orbital gap for osmium tetroxide and ethylene (see section III for all frontier orbital energies). The difference in the energy of the LUMO orbital energies, which is related to the formal reduction potential of the metal, dictates the electrophilicity of the metal oxide and the relative positions of transition state along the reaction coordinate. Ziegler and coworkers have made a similar argument for the low barrier of OsO_4 compared to CrO_2Cl_2.[16d] Deubel and Frenking have also discussed the "wrong" direction of electron follow between Re oxides and ethylene.[16f]

Analysis of the distortion (MO_4 and ethylene) and interaction energies along the (3 + 2) C_s addition pathways from 2.1 to 1.8Å showed similar results compared to the MO_4 angles scans, except the OsO_4 distortion energy is always slightly above the anionic complexes (Figure 10). The three anionic MO_4^- species have nearly identical total distortion energies from 2.1 to 1.8 Å. Importantly, Figure 10 reveals an important aspect of the total interaction energy. At the O−C distance of 2.1 Å only OsO_4 and MnO_4^- additions have stabilizing interactions with ethylene while rhenate and technetate have large destabilizing interactions. At 1.9 Å for TcO_4^- and then 1.8 Å for ReO_4^-, the interaction energies finally become stabilizing. Therefore, the transition state positions correspond to the onset of stabilizing interactions. Section II explores the specific interaction that controls the onset of stabilizing interactions.

II. ALMO-EDA Analysis. To further understand the transition state interaction energies, especially the overall destabilizing interaction in **22TS** and **Mn-32TS**, the absolutely localized molecular orbital energy decomposition analysis (ALMO-EDA)[22,28] was used to decompose the interaction energies into physically

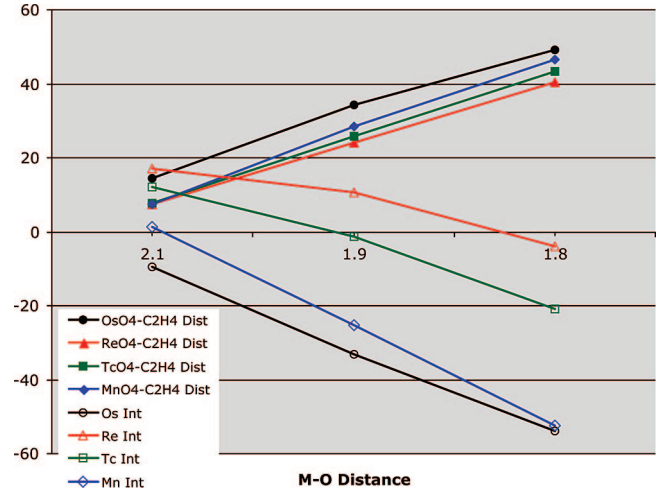

FIGURE 10. OsO_4, ReO_4^-, TcO_4^-, and MnO_4^- comparison of distortion and interaction energies from 2.1 to 1.8Å (kcal/mol).

meaningful terms. These include frozen density ($\Delta E_{(FRZ)}$), polarization ($\Delta E_{(POL)}$), and charge-transfer ($\Delta E_{(CT)}$). $\Delta E_{(FRZ)}$ is the energy change resulting from bringing the metal oxo and ethylene into close proximity in their predistorted transition state geometries without orbital relaxation, a combination of Coulombic and exchange interactions. Because the Coulombic and exchange terms are not properly antisymmetrized in this method they cannot be separated. $\Delta E_{(POL)}$ is a result of intramolecular relaxation of the absolutely localized orbitals due to the presence of the other fragment. The $\Delta E_{(CT)}$ term, dissected into directional contributions, is computed from a difference between localized and delocalized molecular orbital energies with correction for

TABLE 2. Transition State Absolutely Localized Molecular Orbital Interaction Energy Decomposition Results (kcal/mol)

TS	$\Delta E_{(FRZ)}$	$\Delta E_{(POL)}$	$\Delta E_{(CT)}$	$MO_4 \rightarrow C_2H_4$	$C_2H_4 \rightarrow MO_4$	$\Delta E_{(HO)}$	$\Delta E_{(INT)}$
32TS	41.7	−2.4	−61.3	−7.2	−54.1	15.6	−6.4
22TS	89.7	−25.7	−41.8	−17.5	−24.2	−5.5	16.7
NH_3-32TS	46.7	−4.1	−56.5	−8.2	−48.3	10.9	−3.1
NH_3-22TS	86.0	−23.0	−40.9	−16.2	−24.7	−5.6	16.5
Re-32TS	120.5	−15.8	−109.3	−35.2	−74.1	7.6	3.0
Tc-32TS	94.1	−14.4	−75.8	−27.0	−48.8	−0.2	3.7
Mn-32TS	48.5	−5.3	−33.1	−13.0	−20.2	−4.6	5.5

TABLE 3. Reduction Pathway Absolutely Localized Molecular Orbital Interaction Energy Decomposition Results (kcal/mol)

	$\Delta E_{(FRZ)}$	$\Delta E_{(POL)}$	$\Delta E_{(CT)}$	$MO_4 \rightarrow C_2H_4$	$C_2H_4 \rightarrow MO_4$	$\Delta E_{(HO)}$	$\Delta E_{(INT)}$
$OsO_4 + C_2H_4$							
2.1	44.1	−3.3	−62.5	−7.5	−55.0	15.4	−21.7
1.9	83.6	−9.2	−282.7	−16.7	−266.0	179.6	−208.3
1.8[a]							
$ReO_4^- + C_2H_4$							
2.1	53.0	−6.8	−23.8	−12.5	−11.2	−3.2	22.4
1.9	95.4	−14.3	−63.5	−25.8	−37.6	−3.4	17.7
1.8	128.0	−21.7	−115.8	−36.8	−79.0	10.5	−9.5
$TcO_4^- + C_2H_4$							
2.1	52.2	−6.9	−27.6	−12.9	−14.8	−3.8	17.6
1.9	94.5	−14.7	−78.8	−26.9	−51.9	1.0	0.9
1.8	127.2	−22.6	−156.5	−38.0	−118.5	35.4	−51.8
$MnO_4^- + C_2H_4$							
2.1	50.9	−7.7	−35.6	−13.7	−21.9	−4.5	7.6
1.9	92.7	−16.6	−114.4	−29.2	−85.2	16.3	−38.3
1.8[a]							

[a] Not reported because $\Delta E_{(HO)}$ becomes approximately equal to $\Delta E_{(INT)}$.

TABLE 4. Frontier Orbital Energies, Conceptual DFT Parameters, and Singlet-Triplet Gap for MO_4 Ground State Species (eV)

species	HOMO	LUMO	ΔE_{ST}	μ	η	ω
OsO_4	−10.1	−4.1	3.2	7.4	2.7	10.0
ReO_4	−2.9	3.5	4.3	−0.3	3.2	0.0
TcO_4	−2.9	2.6	3.3	0.1	2.7	0.0
MnO_4	−2.4	1.6	1.4	0.4	2.0	0.0

basis set superposition error. This term gives the amount of covalent bonding, largely due to frontier interactions, and is the sum of charge transfer from the metal oxo to ethylene and vice versa. Higher order orbital relaxation effects ($\Delta E_{(HO)}$), which cannot be assigned to either direction of charge-transfer, are also given. The sum of these terms gives the overall ALMO-EDA interaction energy ($\Delta E_{(INT)}$) which differs only slightly from that computed by the distortion/interaction analysis above ($\Delta E_i^{\ddagger}$) due to the larger basis set and superposition error. Table 2 gives the dissection of the interaction energies for the (3 + 2) and (2 + 2) osmium tetroxide and the (3 + 2) rhenate and permanganate transition states.

In the osmium **32TS**, the $\Delta E_{(FRZ)}$ term indicates that exchange repulsions are 41.7 kcal/mol larger than stabilizing electrostatic interactions. Except for the $\Delta E_{(HO)}$ term, all other terms are stabilizing. The stabilizing charge-transfer orbital interactions lead to −61.3 kcal/mol of stability, but are dampended slightly by the $\Delta E_{(HO)}$ term. The $C_2H_4 \rightarrow OsO_4$ charge transfer is −54.1 kcal/mol stabilizing while the opposite direction, $OsO_4 \rightarrow C_2H_4$, results in only −7.2 kcal/mol of stabilizing interaction. The majority of charge-transfer stabilization is the result of the $HOMO_{ethylene}-LUMO_{OsO4}$ interaction. Veldkamp and Frenking have previously reported charge decomposition calculations that also suggested OsO_4 acts as an electrophilic reagent[16] and is confirmed experimentally by Sharpless who reported faster reaction rates for electron rich than electron poor alkenes.[42] In the corresponding amine-catalyzed TS, **NH_3-32TS**, the $\Delta E_{(FRZ)}$ term is 5 kcal/mol more destabilizing and there is ∼5 kcal/mol less stabilizing charge-transfer from $C_2H_4 \rightarrow OsO_4$ leading to approximately half the total stabilizing interaction compared to **32TS**.

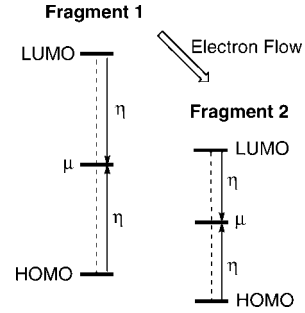

FIGURE 11. Qualitative diagram depicting the HOMO−LUMO gap, chemical potential, and hardness.

Despite the large activation energy for **22TS** compared to **32TS**, this transition state has a total −41.8 kcal/mol of stabilizing charge-transfer. Combined with the stabilizing polarization resulting from the Os−C partial bond ($\Delta E_{(POL)}$) and higher order orbital relaxation ($\Delta E_{(HO)}$), the total orbital interaction terms for **22TS** result in more stabilization than in **32TS**. However, the overall destabilizing $\Delta E_{(INT)}$ is the result of nearly twice the $\Delta E_{(FRZ)}$ term in **22TS** compared to **32TS**. The values for the decomposition terms in **NH_3-22TS** are nearly identical to **22TS**.

The ALMO-EDA method gives overall destabilizing interaction energies for all anionic metal−oxo transition states (**Re-32TS**, **Tc-32TS**, and **Mn-32TS**). This is in contrast to the slightly stabilizing $\Delta E_i^{\ddagger}$ for **Re-32TS** and **Tc-32TS** (−3.1 and −5.7 kcal/mol) computed in section I. The difference is likely due to basis set superposition error in $\Delta E_i^{\ddagger}$ values; $\Delta E_{(INT)}$ is corrected for such error. Despite rhenate being an anionic complex, the charge-transfer ($\Delta E_{(CT)}$) in **Re-32TS** leads to −109.3 kcal/mol of stabilization, which is nearly twice the amount in **32TS**. However, this stabilization is mitigated by a larger $\Delta E_{(FRZ)}$ term of 120.5 kcal/mol. In **Tc-32TS** and **Mn-32TS**, both the charge-transfer and exchange repulsion terms decrease as a result of an earlier transition state.

Because the transition states for MO_4 addition to ethylene occur at different positions along the reaction coordinate we have also computed the ALMO-EDA energies at C−O bond lengths of 2.1, 1.9, and 1.8 Å (Table 3). Despite the difference in charge between OsO_4 and MnO_4^-, the $\Delta E_{(FRZ)}$ values are similar at 2.1 and 1.9 Å. In fact, all three anionic metal oxides have nearly the same $\Delta E_{(FRZ)}$ values from 2.1 to 1.8 Å. Because no metal carbon bond is being formed, the $\Delta E_{(POL)}$ terms also change by similar (small) amounts. A very large change occurs in the $\Delta E_{(CT)}$ terms. For example, for OsO_4 addition to C_2H_4 between 2.1 and 1.9Å, $\Delta\Delta E_{(CT)} = -220$ kcal/mol. This change is almost exclusively due to the ethylene→OsO_4 charge-transfer direction. However, for rhenate addition to ethylene, the change in charge-transfer along the reaction coordinate is much less, $\Delta E_{(CT)} = -24$ kcal/mol at 2.1Å (approximately half the value of osmium tetroxide reaction) and −64 and −115 at 1.9 and

(42) (a) Hentges, S. G.; Sharpless, K. B. *J. Am. Chem. Soc.* **1980**, *102*, 4263. (b) Sharpless, K. B.; Willams, D. R. *Tetrahedron Lett.* **1975**, *35*, 5045.

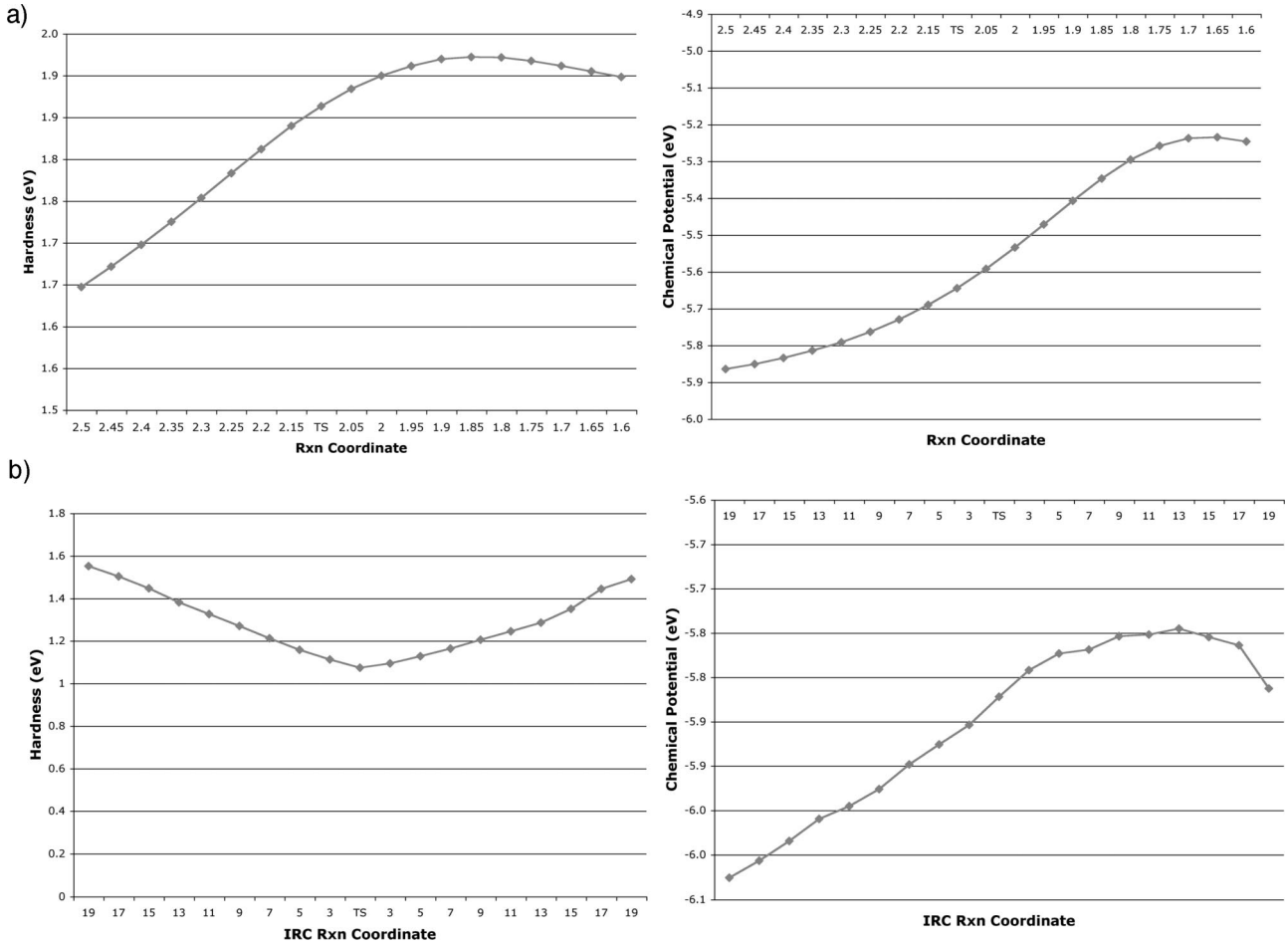

FIGURE 12. Hardness and chemical potential values along the reaction pathways for (a) (3 + 2) addition and (b) (2 + 2) addition.

1.8 Å, respectively. The difference between ReO_4^-, TcO_4^-, and MnO_4^- is the result of ethylene → MO_4^- charge-transfer and controls the position of the transition state along the reaction coordinate. The opposite direction of charge transfer increases at about the same rate for all reactions.

III. Conceptual Density Functional Theory Analysis. Because DFT has become the most widely used quantum mechanical type of calculation, there has been rapid development of quantitative and qualitative reactivity and selectivity DFT-based molecular and reaction descriptors.[43] DFT descriptors are based on electron density properties, such as ionization potentials (IP) and electron affinities (EA) that are independent of molecular orbitals and their symmetries.[44] Although Koopman's theorem is not completely valid in DFT, HOMO (and LUMO) energies are typically invoked to approximate these values.[45] There are two fundamental quantities that are used to derive most of the conceptual DFT descriptors. The first is the chemical potential, $\mu = (\delta E/\delta N)$, which is the tendency of electrons to be transferred to or from a molecule.[46] This quantity is defined as the partial derivative of the energy (E) with respect to the charge, that is, the change in energy of a system with the change in the number of electrons (N) at a constant nuclear geometry. This partial derivative is often approximated as (EA-IP)/2 or (HOMO + LUMO)/2. A large μ value is the result of a highly electronegative molecule resulting in a large ionization potential and a large electron affinity. The second important quantity in conceptual DFT is the hardness, $\eta = 1/2(\delta^2 E/\delta N^2)$, defined as how the chemical potential changes with change in electron number and is the second partial derivative of the chemical potential which is approximated to be (IP-EA)/2 or (LUMO − HOMO)/2.[47] The hardness describes the molecular polarizability. Overall, the interaction between molecules, dissected into soft−soft (charge-transfer) and hard−hard (electron reorganization or electrostatic) interactions, is driven by a difference in chemical potentials (Figure 11).[48]

(43) Ess, D. H.; Jones, G. O.; Houk, K. H. *Adv. Synth. Catal.* **2006**, *348*, 2337.

(44) (a) Pearson, R. G. In *Theoretical Models of Chemical Bonding Part 2 the Concept of the Chemical Bond*; MaksicZ. B., Ed.; Springer-Verlag: Berlin, Heidelberg, 1990. (b) Parr, R. G.; Yang, W. T. *Annu. Rev. Phys. Chem.* **1995**, *46*, 701. (c) Parr, R. G.; Yang, W. In *Density-Functional Theory of Atoms and Molecules*; Oxford UP: New York, 1989. (d) Ayers, P. W.; Anderson, J. S. M.; Bartolotti, L. J *Int. J. Quantum Chem.* **2005**, *101*, 520. (e) Chandrakumar, K. R. S.; Pal, S. *Int. J. Mol. Sci.* **2002**, *3*, 324. (f) Chatttaraj, P. K.; Lee, H.; Parr, R. G. *J. Am. Chem. Soc.* **1991**, *113*, 1855. (g) Parr, R. G.; Chatttaraj, P. K. *J. Am. Chem. Soc.* **1991**, *113*, 1854. (h) Parr, R. G.; Yang, W. *J. Am. Chem. Soc.* **1984**, *106*, 4049. (i) Gázquez, J. L.; Méndez, F. *J. Phys. Chem.* **1994**, *98*, 4591. (j) Geerlings, P.; De Proft, F.; Langenaeker, W. *Chem. Rev.* **2003**, *103*, 1793.

(45) (a) Janak, J. F. *Phys. Rev. B* **1978**, *18*, 7165. (b) Savin, A.; Umrigar, C. J.; Gonze, X. *Chem. Phys. Lett.* **1998**, *288*, 391. (c) For a discussion on the proper use of HOMO and LUMO values in conceptual DFT, see: (d) Ayers, P. W.; De Proft, F.; Borgoo, A.; Geerlings, P. *J. Chem. Phys.* **2007**, *126*, 224107.

(46) Parr, R. G.; Donnelly, R. A.; Levy, M.; Palke, W. E. *J. Chem. Phys.* **1978**, *68*, 3801.

(47) (a) Parr, R. G.; Pearson, R. G. *J. Am. Chem. Soc.* **1983**, *105*, 7512. (b) Ayers, P. W. *Faraday Discuss.* **2007**, *135*, 161.

(48) (a) Parr, R. G.; Gázquez, J. L. *J. Phys. Chem.* **1993**, *97*, 3939. (b) Méndez, F.; Gázquez, J. L. *J. Am. Chem. Soc.* **1994**, *116*, 9298.

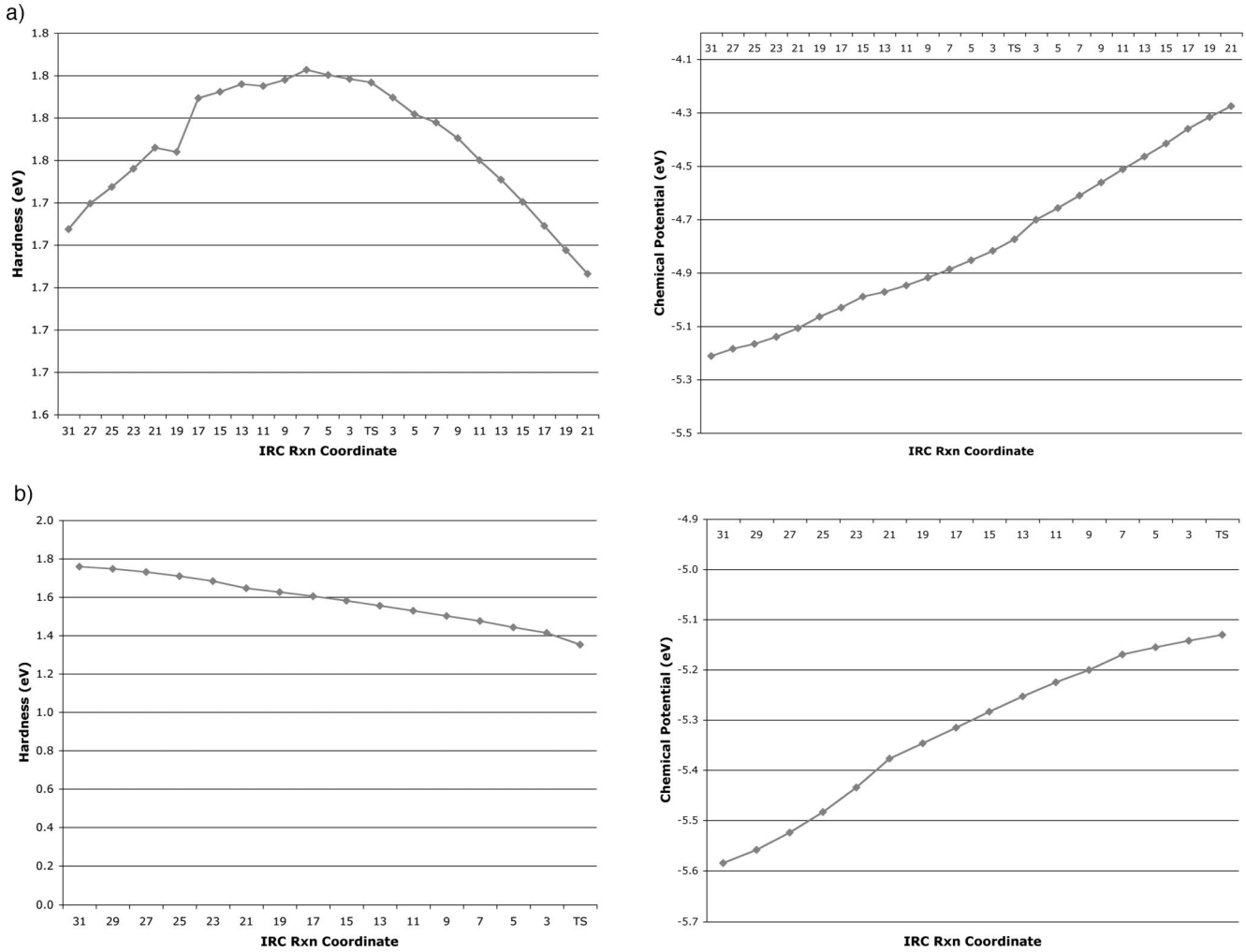

FIGURE 13. Hardness and chemical potential values along the reaction pathways for amine-assisted (a) (3 + 2) addition and (b) (2 + 2) addition.

Another useful descriptor is the so-called "electrophilicity index", ω,[49,50] which has been used as a measure for reactivity for a variety of 1,3-dipolar and Diels−Alder cycloadditions.[51−53] Similar to the electron affinity, $\omega = \mu^2/2\eta$, is a measure of the capability of a molecule to accept electrons and is indicative of a large chemical potential that is dampened by the hardness.[51]

The ALMO-EDA energy decomposition results from section II indicate the transition states involve an electrophilic metal oxo species interacting with ethylene. Table 4 gives the Kohn−Sham orbital energies, the chemical potential, hardness, and electrophilicity for OsO_4, ReO_4^-, TcO_4^-, and MnO_4^-. As expected, the neutral osmium tetroxide has the lowest energy HOMO and LUMO energies giving a large chemical potential of 7.4 eV, indicative of a very powerful electrophile according to the ω scale (10.0 eV). Despite the rhenate transition state having the largest charge-transfer, this anionic species along with technetate and permanganate have chemical potentials and electrophilicity values close to zero.[51]

Recently, De Proft, Ayers, Geerlings, and co-workers have shown that tracking the hardness during the initial stages of a reaction provides equivalent information to the "allowed" and "forbidden" description that are derived from the Woodward−Hoffmann rules based on orbital symmetry.[25] As noted previously, the osmium tetroxide transition states have been classified as forbidden, but metal-catalyzed. Figure 12 shows the change in hardness along the C_s symmetric addition pathway for (3 + 2) addition and the intrinsic reaction coordinate and (2 + 2) addition of osmium tetroxide to ethylene. For the (3 + 2) pathway, Figure 12a, the hardness increases steadily and plateaus just after the TS. This curve is indicative of an allowed reaction because the HOMO−LUMO gap increases, due to proper stabilizing fragment orbitals mixing, along the initial stages of the reaction coordinate. In contrast, the hardness curve for the (2 + 2) reaction shows the characteristic profile of a forbidden reaction. Here the hardness decreases during the initial interaction and comes to a minimum at the TS before increasing back to a value close to the separated reactants. The chemical potential profiles show very similar curvature. For the amine catalyzed reaction (Figure 13), the hardness and chemical potential profiles prior to the TSs are highly similar to those in the uncatalyzed reaction. However, after the TS in the amine-catalyzed (3 + 2)

(49) Maynard, A. T.; Huang, M.; Rice, W. G.; Covell, D. G. *Proc. Natl. Acad. Sci. U.S.A.* **1998**, *95*, 11578.
(50) Parr, R. G.; Szentpály, L. v.; Liu, S. *J. Am. Chem. Soc.* **1999**, *121*, 1922.
(51) Chattaraj, P. K.; Sarkar, U.; Roy, D. R. *Chem. Rev.* **2006**, *106*, 2065.
(52) Pérez, P.; Domingo, L. R.; Aurell, M. J.; Contreras, R. *Tetrahedron* **2003**, *59*, 3117.
(53) Pérez, P.; Domingo, L. R.; Aurell, M. J.; Contreras, R. *Tetrahedron* **2002**, *58*, 4417.

addition, Figure 13a, the hardness decreases rapidly. The chemical potential also increases linearly. These hardness profiles provide definitive "allowed" and "forbidden" descriptions to be assigned to the (3 + 2) and (2 + 2) pathways, without resorting to difficult arguments based on orbital interactions.

Conclusion

The reaction pathways of ethylene cycloaddition to metal tetroxides (OsO_4, ReO_4^-, TcO_4^-, and MnO_4^-) were studied using distortion/interaction, ALMO-EDA, and conceptual DFT analyses. The (2 + 2) transition state activation barrier is ~40 kcal/mol greater than the (3 + 2) transition state because the Os−O bond is stretched significantly resulting in a larger distortion energy and the transition state interaction energy is destabilizing due to large exchange repulsions. Both (3 + 2) and (2 + 2) transition states have significant stabilizing charge-transfer interactions, in accord with frontier orbital expectations. Base ligation lowers osmium tetroxide and ethylene distortion energies due to the ground state O−Os−O angle being predistorted. Reactivity differences between OsO_4, ReO_4^-, TcO_4^-, and MnO_4^- were shown to be a function of ethylene → MO_4 charge-transfer because MO_4 distortion energies are similar. The position of the transition state along the reaction coordinate corresponds to the onset of overall stabilizing interaction energies. Conceptual DFT hardness profiles provided definitive "allowed" and "forbidden" descriptions to be assigned to the (3 + 2) and (2 + 2) OsO_4 cycloaddition ethylene reaction pathways.

Acknowledgment. Professor Thomas Strassner is thanked for a helpful review of this manuscript.

Supporting Information Available: Absolute energies and Cartesian coordinates. Full Q-Chem and Gaussian 03 references. This material is available free of charge via the Internet at http://pubs.acs.org.

JO802189W